Purification of acidic lignocellulose hydrolysate using anion-exchange resin: Multicomponent adsorption, kinetic and thermodynamic study

Jian Han [a, b], Bin Xu [c], Huan Wang [c], Guohong Huang [d], Xiaolei Zhang [e], Yong Xu [a, b*]

[a] *Jiangsu Co-Innovation Center of Efficient Processing and Utilization of Forest Resources, College of Chemical Engineering, Nanjing Forestry University, Nanjing 210037, People's Republic of China*

[b] *Jiangsu Province Key Laboratory of Green Biomass-based Fuels and Chemicals, Nanjing 210037, People's Republic of China*

[c] *ECO Zhuoxin Energy-saving Technology (Shanghai) Company Limited, Shanghai 200000, People's Republic of China*

[d] *Nanjing Hydraulic Research Institute, Materials & Structural Engineering Department, Nanjing 210029, People's Republic of China*

[e] *Department of Chemical and Process Engineering, University of Strathclyde, Glasgow, UK G1 1XJ*

***** Corresponding author at: College of Chemical Engineering, Nanjing Forestry University. No. 159 Longpan Road, Nanjing 210037. People's Republic of China.

E-mail address: xuyong@njfu.edu.cn (Y. X.)

Tel: +86 025 85427587

Fax: +86 025 85427587

Abstract

Acid hydrolysis of lignocellulosic biomass to produce high value-added products presents a breathtaking industrial application foreground. However, the hydrolysate under harsh conditions contains extremely complex degradations, resulting in many restrictions or lethal toxicity on the following utilization and bioconversion. In this study, the anion-exchange resin 335 was exploited to separate and purify main degradations from the acidic corncob-hydrolysate. A comprehensive investigation was explored on equilibrium isotherms, adsorption kinetics, and thermodynamic parameters of the representative substances in the hydrolysate. The results indicated that the removal of acetic acid, furfural, and total lignin derivates reached 90.13%, 92.58%, and 94.85% respectively, while the loss rate of xylose was well controlled within 20%. Based on these studies, various models and parameters were evaluated to uncover the mechanisms. In conclusion, this work offered a theoretical basis for the application in the separation and purification of acidic lignocellulose-hydrolysate and further bioconversion.

Keywords: acidic lignocellulose-hydrolysate, anion-exchange resin, equilibrium isotherms, adsorption kinetics, thermodynamic parameters

1. Introduction

In the context of global carbon neutrality, the traditional inefficient combustion of lignocellulosic biomass is inevitably undesirable (Nitzsche et al., 2019a). Efficient utilization of lignocellulosic resources from such a large amount of agricultural and forestry waste worldwide is an urgent problem to be solved (Wright et al., 2010). Many researchers have indeed conducted a lot of research and attempts in the field of lignocellulosic biorefinery (Guo et al., 2020). The densely structured lignocellulosic biomass, which is mostly made of cellulose, hemicellulose, and lignin must undergo a suitable pretreatment process to release hemicellulose and lignin into liquid fractions as much as possible while retaining cellulose in solid fractions for subsequent hydrolysis to produce glucose (Alriksson et al., 2006). Acid hydrolysis was the most convenient for industrialization due to its rapid, efficiency, and inexpensive characteristics. Acidic hydrolysate typically contains xylose and inhibitors of weak acids, furans, and lignin derivatives (Ma and Yang, 2015). Some of the chemicals that serve as fermentation inhibitors in hydrolysate are active in industrial applications (Huang et al., 2020). Acetic acid (AA), as the highest content of aliphatic organic acid in hemicellulose hydrolysate, is one of the important organic chemical raw materials, widely used in medicine, pesticide synthetic fiber (Sankaranarayanan et al., 2015). Furfural (FF) is a raw material for many pharmaceutical and industrial products and is also used in synthetic resins, pesticides, pharmaceuticals, and rubbers. Lignin derivatives (LG) are widely used in biochemistry and industrial synthesis (Nitzsche et al., 2019b). Xylose (XYL), the main sugar component of hemicellulose hydrolysate, can be used to

synthesize chemical products like xylonic acid and xylitol (You et al., 2019). It is worth mentioning that xylonic acid, as a new multi-functional and multi-purpose platform compound, is considered as one of the 30 most valuable chemicals, and has enormous development and application potential (Zhang et al., 2017). However, the direct utilization of these mixed substances is extremely difficult and challenging, so it is necessary to separate and purify the lignocellulose hydrolysate (Han et al., 2021).

Commonly used techniques for the removal of fermentation inhibitors include solvent extraction (Zhu et al., 2014), membrane filtration (Cao and Xu, 2019), ion exchange (Kumar et al., 2018), and adsorption (Dai et al., 2020). In comparison to other separation processes, adsorption is preferred due to its low cost and high removal efficiency. Activated carbon, as a traditional and widely used adsorbent, has a strong capacity for adsorption, but its application is limited by its relatively pricey, poor selective adsorption, and difficulty in regeneration. Polymer resins have emerged as a viable option for efficiently eliminating fermentation inhibitors due to their excellent adsorption performance, superior selectivity, and ease of regeneration (Yu and Christopher, 2017). Roy Nitzsche determined and applied the adsorption isotherms for removing lignin from wood hydrolysate utilizing polymeric resins (Nitzsche et al., 2019b). You et.al purified hemicellulose from the hydrolysate of bagasse by adsorption resin, and the content of lignin decreased by 89.2% (You et al., 2019).

So far, the research on hydrolysate purification has mainly focused on the removal of lignin, and less attention has been paid to other fermentation inhibitors (Chen et al., 2019). This necessitates a research effort to establish a thorough study of the

84 equilibrium, kinetic and thermodynamic of typical fermentation inhibitors (acetic acid,
85 furfural, and lignin) and fermentable sugar xylose adsorption from lignocellulose
86 hydrolysate (Cao et al., 2020). This is also the main intention of our current work. We
87 first studied the adsorption performance of gel-type anion-exchange resin 335 on the
88 multi-components (acetic acid, furfural, lignin, and xylose) of acidic corncob
89 hydrolysate, and determined the resin adsorption capacity under different parameters
90 (Hua et al., 2020). The standard Langmuir and Freundlich isotherm models were then
91 used to match the equilibrium experiment results (Lin et al., 2017). The adsorption
92 kinetics were also investigated and predicted by the pseudo-first-order model, pseudo-
93 second-order model, and Weber & Morris diffusion model (Kadam et al., 2010). The
94 thermodynamics parameters including the Gibbs free energy ΔG, enthalpy change ΔH,
95 and entropy change ΔS were calculated by Van't Hoff formula (Boparai et al., 2011).
96 The equilibrium, kinetic and thermodynamic experiments were statistically studied to
97 better comprehend the mechanism of various components in the hydrolysate.
98

2. Materials and methods

2.1. Materials

The acidic corncob hydrolysate (ACH) was provided by ECO Zhuoxin Energy-saving Technology Co., Ltd., which contained 55.05 g/L xylose, 8.03 g/L glucose, 10.27 g/L arabinose, 9.51 g/L acetic acid, 3.76 g/L furfural, and 6.33 g/L lignin.

The resin 335 was obtained from Huazhen Technology Co., Ltd. (Shanghai, China). 335 resin is commonly used in the preparation of pure water, sugar refining, organic acid refining, and organic acid neutralization in antibiotic extraction. The functional groups of 335 resin were $-NH_2$, =N, and ≡N. The resin was initially cleaned before its utilization in subsequent experiments. The cleaning process included sequentially soaking with 1 mol/L NaOH, 1 mol/L HCl, and 1 mol/L NaOH in a 30℃ water bath for 2 h, the pH was then adjusted with distilled water until it was close to neutral. The cleaned resin was stored in 1 M NaOH at 4 °C.

2.2 Adsorption on resin

The adsorption behavior of 335 resin on acetic acid, furfural, lignin, and xylose in ACH was investigated under different environmental conditions. The influence of resin dosage was studied at the resin to solution ratios (R: S) of 1:5, 1:10, 1:15, 1:20, 1:30, and 1:40 w/v. In a thermostatic oscillator, the mixture was placed in a 500ml beaker and constantly shaken at 150 rpm for 2 hours at 303K. The influence of initial ACH concentration was investigated at 303, 313, 323, and 333 K. The influence of contact time is determined by intensive sampling during the above experiment. After the sorption, the filtered hydrolysate was analyzed for the instantaneous composition, as

121 described below.

122 **2.3 Analysis methods**

123 The concentrations of xylose, acetic acid, and furfural were all analyzed using high-
124 performance liquid chromatography. Elution was conducted at a flow rate of 0.6
125 mL/min using 5.0 mM sulfuric acid (Zhou et al., 2018).

126 Lignin content was quantified by the absorption at 280 nm, using a UV/VIS
127 spectrophotometer with a 1 cm quartz cuvette (Nitzsche et al., 2019b). The solution was
128 diluted with deionized water to keep the absorbance in the range of 0.3 to 1.0. The lignin
129 concentration was calculated with Eq. (1):

130 $$C_{lignin} = \frac{A_{280} D}{\alpha L} \quad (1)$$

131 A_{280} denotes the absorbance at 280 nm, D denotes the dilute times, α is the extinction
132 coefficient (110 L/g·cm as an average value) and L is the quartz cuvette width (1 cm).
133 The removal rate of xylose and fermentation inhibitors from ACH was calculated using
134 Eq. (2):

135 $$\text{Removal rate}(\%) = \frac{C_0 - C_e}{C_0} \times 100 \quad (2)$$

136 C_0 and C_e represent the initial and equilibrium concentration (g/L).

137 The adsorption capacity Q_e (mg/g) was computed as the following Eq. (3):

138 $$Q_e = \frac{(C_0 - C_e)V}{m} \quad (3)$$

139 V refers to the solution volume (mL), while m to the mass of dry adsorbent (g).

140

3. Results and discussion

3.1. Effect of adsorption process parameters on the removal of multi-components in hydrolysate

Figuring out the removal of multi-components from lignocellulosic hydrolysate with different adsorption process parameters is an important basis for understanding the adsorption mechanism of various components in hydrolysate (Lee et al., 2015). Thus, the removal rates of XYL, AA, FF, and LG in ACH were firstly studied under different conditions, and the results were shown in Fig. 1. With a higher R: S ratio, the elimination rate of XYL, AA, FF, and LG rises. At the R: S ratio of 1:5, the maximal removal rate of AA, FF, and LG was 90.13%, 92.58%, and 94.85%, respectively. Correspondingly, the loss rate of xylose reached a maximum of 19.09%. It can be reasonably inferred from the curves on the graph that AA, FF, and LG can be completely removed from ACH theoretically with the further improvement of the R: S ratio. Of course, the loss rate of xylose will also be further improved. We believe that the loss within 20% is an acceptable range, so the optimal R: S ratio is determined as 1:5.

To explore the influence of different initial concentrations on the adsorption process, the experiment of ACH with different dilution ratios was carried out at the R: S ratio of 1:10. 1:5 was not selected because the removal rate of various components in diluted ACH was close to 100% under this condition, so it was unachievable to analyze the impact of various initial concentrations. Anyway, it can be seen from Fig. 1 that with the increase of dilution ratio which means the decrease of initial

concentration, the removal rates of XYL, AA, FF, and LG are getting higher. This is an interesting phenomenon from a resin adsorption perspective, in general, the removal rate of a substance increases as its initial concentration increases. We infer that it may be because deionized water dilution is also a purification step of ACH. 335 resin is more capable of treating purified hydrolysate, and the relative removal rate increases as the initial substrate concentration decrease. The kinetic curve showed that the removal rates of XYL, AA, FF, and LG were divided into a rapid and slow increase stage. Following that, as adsorption time passed, the concentration fell until it reached equilibrium. FF and LG reached equilibrium at about 40 minutes, AA and XYL reached equilibrium at 60 minutes and 90 minutes, respectively. This difference is reflected in the selective adsorption of the resin. The weak base epoxy resin 335 has strong adsorption for aromatic and weak acid molecules compared with sugars.

The influence of temperature was studied using an initial hydrolysate at 303, 313, 323, and 333K. As seen in Fig. 1, the removal rates of XYL, AA, FF, and LG in ACH increased with the increase of temperature. This phenomenon may be related to the different diffusion rates and solubility in solution at different temperatures, and their adsorption process may be an endothermic reaction. The final proof can be obtained through subsequent thermodynamic studies.

3.2. Equilibrium isotherm models

The equilibrium isotherm model predicted by the adsorption behavior of a specific adsorbent is crucial to understanding the mechanism of the adsorption process. The composition of hydrolysate is very complex and the specific influence of these

complex components on the adsorption process is unclear(Chowdhury et al., 2014). Therefore, the adsorption process of the model solution containing single xylose, acetic acid, furfural, phenol, and their mixture on 335 resin was examined, and the outcomes are shown in Figure 2. It can be observed that the removal rates of xylose, acetic acid, and furfural are very similar in the mixed solution and the single component model solution, except for phenol. It may be because the UV absorption peaks of furfural and phenol are close, which affects the determination of phenol content. Anyway, it can be concluded that in the model solution, the interaction and/or competition is slight for the adsorption on 335 resin between the various components. Regardless of the complexity of the adsorption process of various components in lignocellulosic hydrolysate, simple models can offer some insight into the factors that determine the adsorption of sugars and fermentation inhibitors. Here we used two of the most typical and commonly used equilibrium adsorption models, the Langmuir and Freundlich models (Senthil Kumar et al., 2010). Based on the fact that intermolecular forces diminish fast as distance increases, the Langmuir model adopts the following assumptions: the surface of the adsorbent is uniform and the adsorption occurs at the monolayer. The interaction of the adsorbed molecules is insignificant (Marczewski and Adam, 2010). It can be represented as the Eq. (4):

$$Q_e = \frac{Q_{max} K_L C_e}{1 + K_L C_e} \tag{4}$$

And by deforming Eq. (4), we can derive the linear equation (5). :

$$\frac{C_e}{Q_e} = \frac{1}{K_L Q_{max}} + \frac{C_e}{Q_{max}} \tag{5}$$

Where K_L is Langmuir constant ($L \cdot g^{-1}$), Q_{max} is the maximal equilibrium adsorption

capacity ($mg \cdot g^{-1}$);

The Freundlich model describes a non-ideal adsorption system and may be used to multilayer adsorption on non-uniform adsorbent surfaces (Qiu et al., 2013). And it can be expressed as the following:

$$Q_e = K_F {C_e}^{1/n} \quad (6)$$

After linearization, we can get Eq. (7):

$$\mathrm{In}Q_e = InK_F + \frac{1}{n}InC_e \quad (7)$$

Where K_F and n are the Freundlich constants.

Figure 3 depicts the experimental data as well as the fitted Langmuir and Freundlich models for XYL, AA, FF, and LG adsorption onto 335 resin. Table S1 summarizes the particular parameters of the two models. Within a certain range, both the Langmuir and Freundlich models can accurately predict the adsorption of XYL, AA, FF, and LG, but in general, the Langmuir model has a better fitting according to the higher R^2 value. This suggests that the adsorption process on the 335 resin is monolayer adsorption, with slight interaction between adsorbents which was already shown in the model solution. K_L value represents the interaction between adsorbent and adsorbent. According to the K_L value shown in Table S1 (Supplementary Materials), the sequence of the interaction strength between the various substances in ACH and adsorbent can be inferred as FF > LG > AA > XYL. This also explains why the removal rate of fermentation inhibitors (AA, FF, and LG) is much higher than that of sugars (XYL), which reflects the selective adsorption capacity of 335 resin. Moreover, the n values of Freundlich model for the four substances are all between 0

229 and 10, suggesting that the adsorption behavior is beneficial and reversible.

230

231 **3.3. Adsorption kinetic model**

232 Adsorption kinetics, which can be used to forecast the rate of adsorption equilibrium,
233 is significant in understanding the adsorption mechanism (A et al., 2010). The
234 standard models for analyzing adsorption kinetics include the pseudo-first-order
235 (PFO), pseudo-second-order (PSO), and Weber&Morris diffusion models (WMD),
236 which are mostly used to estimate the rate control stages of material transfer and
237 physicochemical reaction during adsorption. (Liu and Zhang, 2015).

238 PFO is built based on Lagergren's first-order rate Eq. (8).

239 $$\frac{dQ_t}{dt} = k_1(Q_e - Q_t) \quad (8)$$

240 With the boundary conditions from t = 0 to t = t, the integration of Eq. 8 yields the
241 following equation:

242 $$\mathrm{In}(Q_e - Q_t) = \mathrm{In}Q_e - k_1 t \quad (9)$$

243 $$Q_t = Q_e(1 - e^{-k_1 t}) \quad (10)$$

244 Where k_1 denotes the PFO rate constant (min^{-1}), and Q_t denotes the adsorption
245 capacity at t min ($mg \cdot g^{-1}$).

246 PSO is introduced by Ho and McKay, and its linear expression is as follows:

247 $$\frac{t}{Q_t} = \frac{1}{k_2 Q_e^{\,2}} + \frac{1}{Q_e} t \quad (11)$$

248 Where k_2 denotes the PSO rate constant ($g^{-1} \cdot mg^{-1} \cdot min^{-1}$).

249 WMD was used to identify the primary rate-limiting steps of the adsorption process is
250 as follows:

251 $$Q_t = k_3 t^{1/2} + C \quad (12)$$

Where k_3 denotes the internal diffusion rate constant ($mg \cdot g^{-1} \cdot min^{1/2}$), and C is the constant ($mg \cdot g^{-1}$).

The experimental data and the fitting curves and related parameters of the three adsorption kinetic models are shown in Fig.4 and Table S2 (Supplementary Materials). According to Fig. 4(a), the PSO provides the best match compared with the PFO. Moreover, it also indicated that the PSO is more appropriate due to its higher R^2 in Table S2 (R^2 values are all above 0.99). The maximum equilibrium adsorption capacity predicted by PSO is fairly close to the experimental maximum adsorption capacity. The PSO believes that the adsorption reaction is a rate control step, which is related to the electron transfer and electron sharing between adsorbent and adsorbate. The adsorption process of adsorbate on the adsorbent porous surface is divided into three continuous processes (Mohammadi et al., 2011): (1) Adsorbate transport to the adsorbent's external surface (liquid film diffusion); (2) Adsorbate transport in the adsorbent's pores (intra-particle diffusion); (3) Adsorbate adsorption on the adsorbent's surface. In general, liquid film diffusion or intra-particle diffusion is the rate-limiting step due to the rapid occurrence of the process (3). The fitting lines shown in Fig. 4(b) do not intersect at the origin, indicating that intra-particle diffusion is not the sole rate-limiting process, and that liquid film diffusion and surface adsorption both have an impact on the adsorption rate.

3.4. Absorption thermodynamics

The following formula was used to compute the free energy change ΔG, the enthalpy change ΔH, and the entropy change ΔS of XYL, AA, FF, and LG sorption on 335 resin

(Chen et al., 2011):

$$k_d = \frac{(C_0 - C_e)V}{C_e m} \quad (13)$$

$$\mathrm{In}k_d = \frac{\Delta S}{R} - \frac{\Delta H}{RT} \quad (14)$$

$$\Delta G = -\mathrm{RTIn}k_d \quad (15)$$

k_d is the sorption equilibrium constant (L•g-1) and R is the gas constant 8.314 (J·mol^{-1}·K^{-1}). The slope and intercept of linear Van't Hoff Eq. 14 are used to calculate ΔH and ΔS (Fig.5). Table 1 listed all of the thermodynamic parameters. At the chosen experimental temperature, the values of ΔG are negative, confirming the spontaneous nature of adsorption and the technique's viability. Furthermore, ΔG values are less than 20 kJ·mol^{-1}, manifesting that physical adsorption is the dominant process. The positive ΔH values confirm the adsorption of XYL, AA, FF, and LG onto 335 resin is an endothermic reaction while the positive ΔS reflects the process as an entropy increasing process (Biadasz et al., 2011).

4. Conclusion

The separation of AA, FF, and LG from acidic corncob hydrolysate by resin 335 was systematically investigated. The AA, FF, and LG removal rates reach 90.13%, 92.58%, and 94.85% respectively. Analysis of adsorption isotherms shows that the equilibrium data are fitting the Langmuir isotherm model well. The kinetics investigation revealed that the pseudo-second-order model best describes the sorption process of fermentation inhibitors. According to the thermodynamic analysis, the adsorption process was spontaneous and endothermic. This research identifies a viable adsorbent for purifying lignocellulose hydrolysate as well as a critical theoretical foundation for the whole method.

Acknowledgements

The research was supported by the National Natural Science Foundation of China (32171730) and the Key Research and Development Program of Jiangsu (BE2015758). Also, the authors gratefully acknowledge financial support from the Priority Academic Program Development of Jiangsu Higher Education Institutions.

References:

1. A, L.W., A, L.Y., A, Y.L., A, Y.Z., A, X.M., B, Z.Y., 2010. Study on adsorption mechanism of Pb(II) and Cu(II) in aqueous solution using PS-EDTA resin. Chemical Engineering Journal 163, 364–372.
2. Alriksson, B., Sjöde, A., Nilvebrant, N.-O., Jönsson, L.J., 2006. Optimal conditions for alkaline detoxification of dilute-acid lignocellulose hydrolysates. Applied Biochemistry and Biotechnology 129, 13.
3. Biadasz, A., Bursa, B., Barszcz, B., Bogucki, A., Laskowska, B., Graja, A., D Wróbel, 2011. Thermodynamics and in-situ absorption of Langmuir monolayers of selected copper phthalocyanine substituted with different peripheral groups. Dyes & Pigments 89, 86–92.
4. Boparai, H.K., Joseph, M., O'Carroll, D.M., 2011. Kinetics and thermodynamics of cadmium ion removal by adsorption onto nano zerovalent iron particles. Journal of Hazardous Materials 186, 458–465.
5. Cao, R., Guo, J., Hua, X., Xu, Y., 2020. Investigation on decolorization kinetics and thermodynamics of lignocellulosic xylooligosaccharides by highly selective adsorption with Amberlite XAD-16N. Food Chemistry 310, 125934.
6. Cao, R., Xu, Y., 2019. Efficient Preparation of Xylonic Acid from Xylonate Fermentation Broth by Bipolar Membrane Electrodialysis. Appl Biochem Biotechnol 187, 396–406.
7. Chen, L., Gao, B., Lu, S., Dong, Y., 2011. Sorption study of radionickel on attapulgite as a function of pH, ionic strength and temperature. J Radioanal Nucl

328 Chem 288, 851–858.
329 8. Chen, Xue-fang, Zhang, L., Huang, C., Xiong, L., Li, H., Wang, C., Zhao, C.,
330 Huang, Q., Chen, Xin-de, 2019. Adsorption Study of Acid Soluble Lignin
331 Removal from Sugarcane Bagasse Hydrolysate by a Self-Synthesized Resin for
332 Lipid Production. Appl Biochem Biotechnol 188, 585–601.
333 9. Chowdhury, Z., Zain, S.M., Rashid, A.K., 2014. Equilibrium Isotherm Modeling,
334 Kinetics and Thermodynamics Study for Removal of Lead from Waste Water.
335 Journal of Chemistry 8, 333–339.
336 10. Dai, L., Jiang, W., Zhou, X., Xu, Y., 2020. Enhancement in xylonate production
337 from hemicellulose pre-hydrolysate by powdered activated carbon treatment.
338 Bioresource Technology 316, 123944.
339 11. Guo, J., Cao, R., Huang, K., Xu, Y., 2020. Comparison of selective acidolysis of
340 xylan and enzymatic hydrolysability of cellulose in various lignocellulosic
341 materials by a novel xylonic acid catalysis method. Bioresource Technology 304,
342 122943.
343 12. Han, J., Hua, X., Zhou, X., Xu, B., Wang, H., Huang, G., Xu, Y., 2021. A cost-
344 practical cell-recycling process for xylonic acid bioproduction from acidic
345 lignocellulosic hydrolysate with whole-cell catalysis of Gluconobacter oxydans.
346 Bioresource Technology 333, 125157.
347 13. Hua, X., Du, G., Zhou, X., Nawaz, A., ul Haq, I., Xu, Y., 2020. A techno-practical
348 method for overcoming the biotoxicity and volatility obstacles of butanol and
349 butyric acid during whole-cell catalysis by Gluconobacter oxydans. Biotechnol

Biofuels 13, 102.

14. Huang, C., Zheng, Y., Lin, W., Shi, Y., Huang, G., Yong, Q., 2020. Removal of fermentation inhibitors from pre-hydrolysis liquor using polystyrene divinylbenzene resin. Biotechnology for Biofuels 13, 188.
15. Kadam, K.L., Rydholm, E.C., Mcmillan, J.D., 2010. Development and Validation of a Kinetic Model for Enzymatic Saccharification of Lignocellulosic Biomass. Biotechnology Progress 20, 698–705.
16. Kumar, V., Krishania, M., Preet Sandhu, P., Ahluwalia, V., Gnansounou, E., Sangwan, R.S., 2018. Efficient detoxification of corn cob hydrolysate with ion-exchange resins for enhanced xylitol production by Candida tropicalis MTCC 6192. Bioresource Technology 251, 416–419.
17. Lee, K.M., Kim, K.Y., Choi, O., Woo, H.M., Kim, Y., Han, S.O., Sang, B.I., Um, Y., 2015. In situ detoxification of lignocellulosic hydrolysate using a surfactant for butyric acid production by Clostridium tyrobutyricum ATCC 25755. PROCESS BIOCHEMISTRY 50, 630–635.
18. Lin, X., Huang, Q., Qi, G., Xiong, L., Huang, C., Chen, Xuefang, Li, H., Chen, Xinde, 2017. Adsorption behavior of levulinic acid onto microporous hyper-cross-linked polymers in aqueous solution: Equilibrium, thermodynamic, kinetic simulation and fixed-bed column studies. Chemosphere 171, 231–239.
19. Liu, X., Zhang, L., 2015. Removal of phosphate anions using the modified chitosan beads: Adsorption kinetic, isotherm and mechanism studies. Powder Technology 277, 112–119.

372 20. Ma, L.Y., Yang, X.W., 2015. Six new dammarane-type triterpenes from acidic
373 hydrolysate of the stems-leaves of Panax ginseng and their inhibitory–activities
374 against three human cancer cell lines. Phytochemistry Letters 13, 406–412.
375 21. Marczewski, Adam, W., 2010. Analysis of kinetic Langmuir model. Part I:
376 Integrated kinetic Langmuir equation (IKL): a new complete analytical solution
377 of the Langmuir rate equation. Langmuir the Acs Journal of Surfaces & Colloids
378 26, 15229–38.
379 22. Mohammadi, N., Khani, H., Gupta, V.K., Amereh, E., Agarwal, S., 2011.
380 Adsorption process of methyl orange dye onto mesoporous carbon material-
381 kinetic and thermodynamic studies. Journal of Colloid and Interface Science 362,
382 457–462.
383 23. Nitzsche, R., Gröngröft, A., Kraume, M., 2019a. Separation of lignin from beech
384 wood hydrolysate using polymeric resins and zeolites – Determination and
385 application of adsorption isotherms. Separation and Purification Technology 209,
386 491–502.
387 24. Nitzsche, R., Gröngröft, A., Kraume, M., 2019b. Separation of lignin from beech
388 wood hydrolysate using polymeric resins and zeolites – Determination and
389 application of adsorption isotherms. Separation and Purification Technology 209,
390 491–502.
391 25. Qiu, H., Vijver, M.G., He, E., Peijnenburg, W., 2013. Predicting Copper Toxicity
392 to Different Earthworm Species Using a Multicomponent Freundlich Model.
393 Environmental Science & Technology 47, 4796–4803.

26. Sankaranarayanan, R., Wesley, R., Somanathan, T., Dhakad, N., Shyamalakumary, B., Amma, N.S., Parkin, D.M., Nair, M.K., 2015. Visual inspection of the uterine cervix after the application of acetic acid in the detection of cervical carcinoma and its precursors. Cancer 83, 2150–2156.
27. Senthil Kumar, P., Ramalingam, S., Senthamarai, C., Niranjanaa, M., Vijayalakshmi, P., Sivanesan, S., 2010. Adsorption of dye from aqueous solution by cashew nut shell: Studies on equilibrium isotherm, kinetics and thermodynamics of interactions. Desalination 261, 52–60.
28. Wright, M.M., Daugaard, D.E., Satrio, J.A., Brown, R.C., 2010. Techno-economic analysis of biomass fast pyrolysis to transportation fuels. Fuel 89, S2–S10.
29. You, X., Wang, X., Liang, C., Liu, X., Wang, S., 2019. Purification of hemicellulose from sugarcane bagasse alkaline hydrolysate using an aromatic-selective adsorption resin. Carbohydrate Polymers 225, 115216.
30. Yu, Y., Christopher, L.P., 2017. Detoxification of hemicellulose-rich poplar hydrolysate by polymeric resins for improved ethanol fermentability. Fuel 203, 187–196.
31. Zhang, H., Han, X., Wei, C., Bao, J., 2017. Oxidative production of xylonic acid using xylose in distillation stillage of cellulosic ethanol fermentation broth by Gluconobacter oxydans. Bioresource Technology 224, 573–580.
32. Zhou, Xin, Zhou, Xuelian, Tang, X., Xu, Y., 2018. Process for calcium xylonate production as a concrete admixture derived from in-situ fermentation of wheat

straw pre-hydrolysate. Bioresource Technology 261, 288–293.

33. Zhu, J., Zhu, Y., Zhang, L., Yong, Q., Xu, Y., Li, X., Lian, Z., Yu, S., 2014. Sodium hydroxide regeneration of trialkylamine extractant containing inhibitors from corn stover prehydrolyzate by liquid–liquid extraction. Separation and Purification Technology 126, 39–43.

437 **Table 1**

	Temperature/ K	K_d	△G/kJ mol^{-1}	△H/ kJ mol^{-1}	△S/ kJ mol^{-1}	R^2
Xylose	303	1.103	-0.247	13.584	0.046	0.981
	313	1.279	-0.641			
	323	1.601	-1.263			
	333	1.755	-1.557			
Acetic acid	303	37.674	-9.142	9.899	0.063	0.977
	313	40.474	-9.630			
	323	47.039	-10.341			
	333	53.170	-11.001			
Furfural	303	9.174	-5.583	11.672	0.057	0.978
	313	10.332	-6.077			
	323	11.629	-6.589			
	333	14.048	-7.316			
Lignin	303	12.253	-6.312	7.181	0.044	0.994
	313	13.159	-6.706			
	323	14.528	-7.186			
	333	15.777	-7.637			

438

439

440 **Figure. 1**

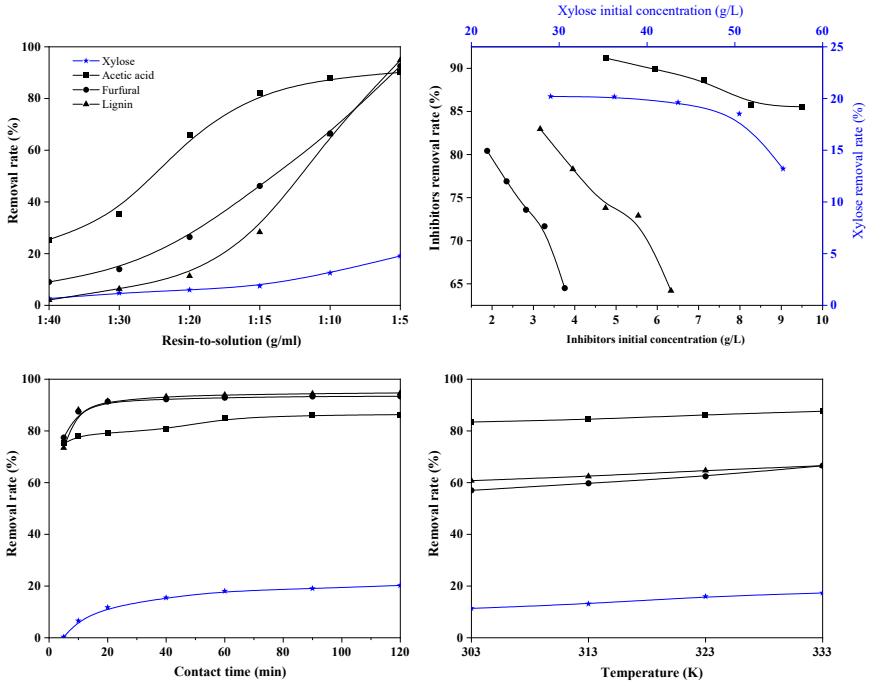

441
442

443 **Figure. 2**

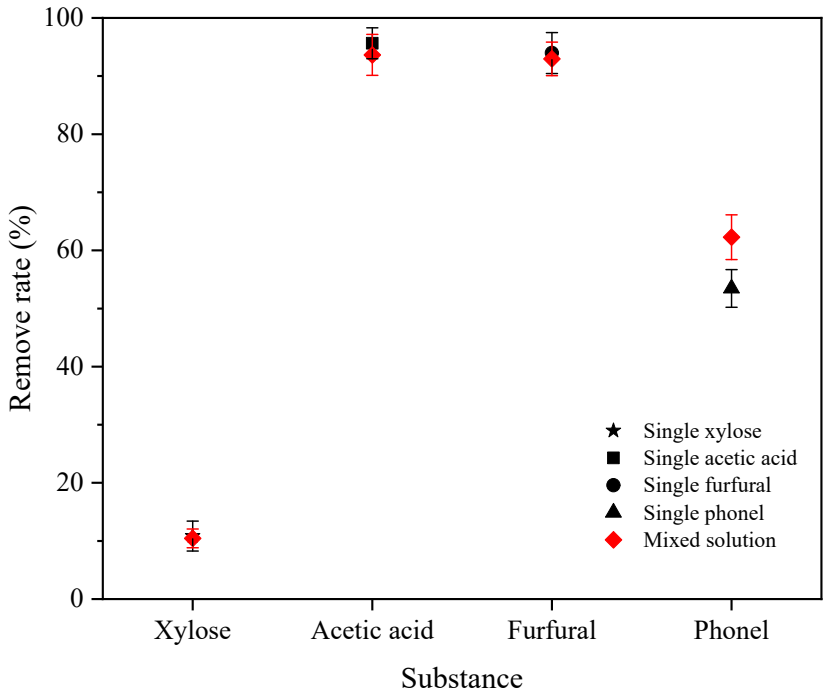

444

445

446

447 **Figure. 3**

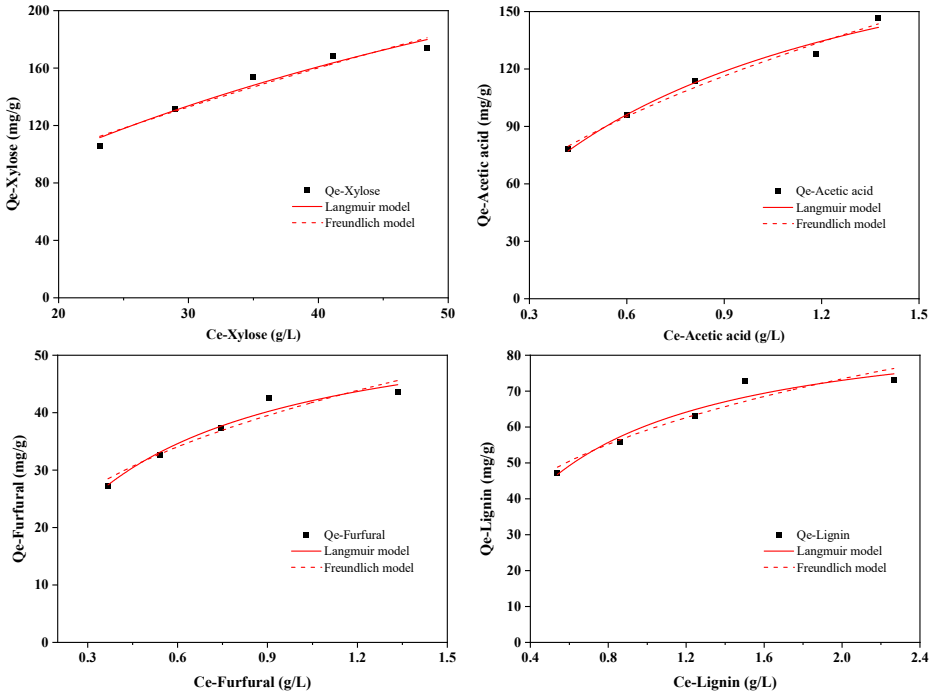

448
449

450 **Figure. 4**

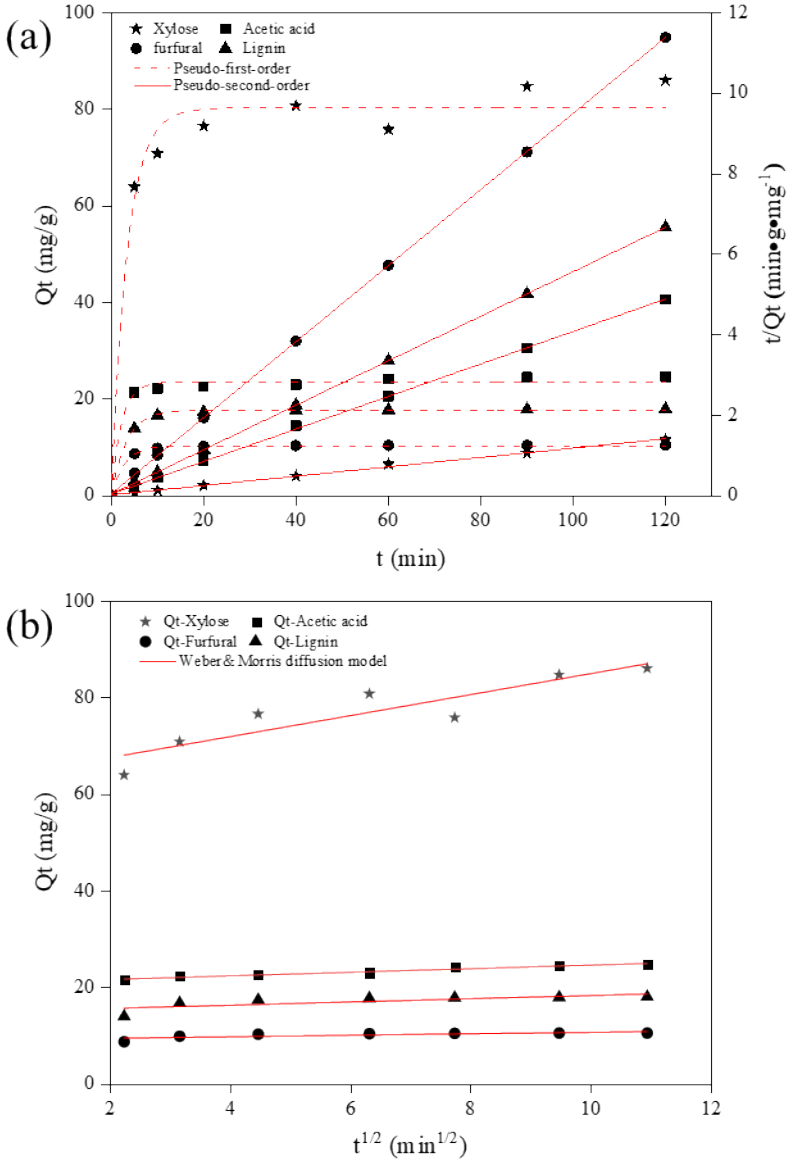

451

452

453 **Figure. 5**

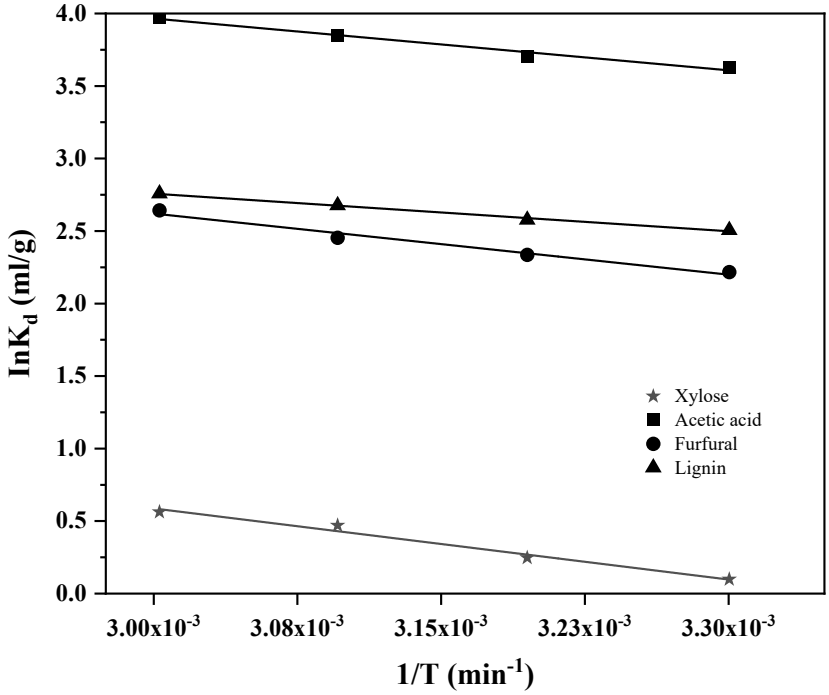

454